Evidence of biological activity in Hawaiian subsurface basalts

M. R. Fisk
College of Oceanic and Atmospheric Sciences, Oregon State University, Corvallis, Oregon, USA
(mfisk@coas.oregonstate.edu)

M. C. Storrie-Lombardi,
Kinohi Institute, Pasadena, California, USA

S. Douglas
NASA Astrobiology Institute, Jet Propulsion Laboratory, California Institute of Technology, Pasadena, California, USA

R. Popa
Department of Earth Sciences, University of Southern California, Los Angeles, California, USA

G. McDonald
NASA Astrobiology Institute, Jet Propulsion Laboratory, California Institute of Technology, Pasadena, California, USA

C. Di Meo-Savoie
College of Oceanic and Atmospheric Sciences, Oregon State University, Corvallis, Oregon, USA

Marine Biomedicine and Environmental Science, Medical University of South Carolina, Charleston, South Carolina, USA

[1] The Hawaii Scientific Drilling Program (HSDP) cored and recovered igneous rock from the surface to a depth of 3109 m near Hilo, Hawaii. Much of the deeper parts of the hole is composed of hyaloclastite (fractured basalt glass that has been cemented in situ with secondary minerals). Some hyaloclastite units have been altered in a manner attributed to microorganisms in volcanic rocks. Samples from one such unit (1336 m to 1404 m below sea level) were examined to test the hypothesis that the alteration was associated with microorganisms. Deep ultraviolet native fluorescence and resonance Raman spectroscopy indicate that nucleic acids and aromatic amino acids are present in clay inside spherical cavities (vesicles) within basalt glass. Chemical mapping shows that phosphorus and carbon were enriched at the boundary between the clay and volcanic glass of the vesicles. Environmental scanning electron microscopy (ESEM) reveals two to three micrometer coccoid structures in these same boundaries. ESEM-linked energy dispersive spectroscopy demonstrated carbon, phosphorous, chloride, and magnesium in these bodies significantly differing from unoccupied neighboring regions of basalt. These observations taken together indicate the presence of microorganisms at the boundary between primary volcanic glass and secondary clays. Amino acids and nucleic acids were extracted from bulk samples of the hyaloclastite unit. Amino acid abundance was low, and if the amino acids are derived from microorganisms in the rock, then there are less than 100,000 cells per gram of rock. Most nucleic acid sequences extracted from the unit were closely related to sequences of Crenarchaeota collected from the subsurface of the ocean floor.

1. Introduction

[2] Microorganisms in subsurface environments may comprise a significant fraction of the Earth's biomass with estimates varying from 5% to 50% [*Parkes et al.*, 1994; *Gold*, 1992; *Whitman et al.*, 1998]. Some of this subsurface biomass consists of microorganisms in igneous rocks both on land and in the oceans. The vast amount of igneous rock on Earth can house a significant amount of biomass even if the concentration of microbes in these rocks is low.

[3] Evidence of microbial activity in igneous rocks was initially described in an outcrop of hyaloclastite from an Icelandic subglacial eruption [*Thorseth et al.*, 1992]. Further evidence of microorganisms has now been recovered from subsurface igneous rocks on land and in the oceans [*Stevens and McKinley*, 1995; *Thorseth et al.*, 1995; *Furnes et al.*, 1996, 2001; *Furnes and Staudigel*, 1999; *Fisk et al.*, 1998; *Giovannoni et al.*, 1996]. It appears that microorganisms have been active in most glassy volcanic rocks of the ocean basins [*Fisk et al.*, 1998; *Furnes et al.*, 2001], and the primary location of bacterial activity in these igneous rocks appears to be in the glass.

[4] Abiotic alteration of volcanic glass produces smooth alteration fronts [see *Fisk et al.*, 1998, Figure 1a] along which glass is transformed to hydrous silicates (palagonite, clay, and iron oxyhydroxides). This chemical alteration is unlike biologically altered glass which has distinctive pits and tubes which produce an irregular boundary between glass and palagonite [*Thorseth et al.*, 1992, 1995; *Fisk et al.*, 1998; *Furnes et al.*, 1999, 2001]. Tubes may be single or branched, smooth-walled or have an irregular granular or pitted surface, they can extend up to 200 μm into the basalt glass, and in some cases contain cell-like

bodies. Different styles of tubes and pits (microbial textures) may occur in close proximity (less than 100 μm from each other). These "microbial" textures can be identified with either optical microscopy [*Fisk et al.*, 1998; *Furnes and Staudigel*, 1999; *Furnes et al.*, 2001] or electron microscopy [*Torsvik et al.*, 1998; *Fisk et al.*, 2000]. Once areas of suspected microbial activity in a rock have been identified by microscopic inspection of petrographic thin sections, tests of microbial activity can then be directed at the areas of interest. Tests for evidence for microbial activity were made on subsurface glassy rocks from Hawaii.

[5] The Hawaii Scientific Drilling Program [*Stolper et al.*, 1996, 2000] drilled a three-kilometer deep hole just outside Hilo, Hawaii (Figure 1a). The hole started in lavas from Mauna Loa volcano and entered lavas from Mauna Kea at 257 m below the surface (Figure 1b). The ages of the lavas range from a few thousand years at the surface [*Lockwood and Lipman*, 1987] to 500,000 to 600,000 years at a depth of the 3000 m [*Stolper et al.*, 2000].

[6] The lavas can be separated into subaerial and submarine eruptions on the basis of lava morphology [*Hawaii Scientific Drilling Project-2*, 2000]. Lava flows make up most of the upper 1080 m (Figure 1c) as indicated by weathered flow tops and sand or soil between the flows [*Moore et al.*, 1996; *Sharp et al.*, 1996]. These lavas are presently below sea level due to subsidence of the island. Lavas deeper than 1080 m depth erupted directly into the ocean resulting in the formation of deposits of fractured basalt glass (hyaloclastites) and pillow basalts. Hyaloclastites make up about half of the section of the hole between 1080 m and the bottom of the hole (Figure 1c). Large volumes of hyaloclastites may be typical of the margins of volcanic islands, because where the margins of Hawaii and
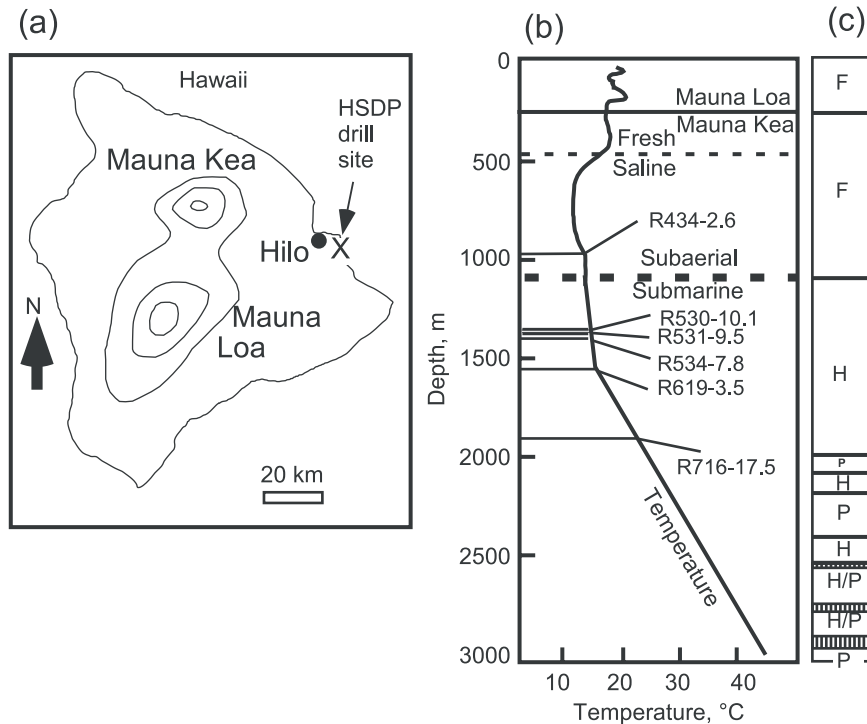
Figure 1. (a) Location of HSDP hole, X. (b) Profile of HSDP. The solid horizontal line is the boundary between Mauna Loa and Mauna Kea lavas. The horizontal thin dashed line is the fresh - saline water boundary. The thick dashed line is the transition from subaerial to submarine eruptions. Temperatures from *Thomas* [2000]. Samples mentioned in this study are identified with an R prefix. (c) Major lithologic units. F lava flows; H hyaloclastites; P pillow basalts; vertical ruled, intrusions. Depths are m below sea level. Modified from *Hawaii Scientific Drilling Project-2* [2000].

other islands in the Hawaiian chain are exposed in the headwalls of landslides, thick deposits of hyaloclastites are found [*Clague and Moore*, 2002].

[7] Temperatures in all sections of the HSDP drill hole are within the range suitable for microorganisms. From the surface to 600 m the temperature decreases from 16°C to 10°C (Figure 1b). This decrease is similar to the temperature profile in the Pacific Ocean near Hilo [*Thomas et al.*, 1996; *Thomas*, 2000] and suggests circulation of seawater to depths of 600 m. Between 600 m and 1600 m the temperature increases to about 15°C and then increases at rate of 20°C/km to 45°C at 3000 m. Thus temperatures in the drill hole are suitable for mesophilic (10 to 45°C) microorganisms. The unit examined in detail in this study was at a temperature of 15°C. Heterotrophic and autotrophic microbial ecosystems could be supported at this temperature by the circulation of fresh or salt water which would contribute organic matter and inorganic oxidants and reductants.

[8] Fluid flow in the volcanic edifice is indicated by the depressed or negative temperature gradient in the upper 1600 m of the HSDP site. Artesian flow in the open drill hole indicates hydraulic pressure is capable of forcing fluids through the porous formation. Down to 470 m the aquifers are fresh (Figure 1b), and below 470 m they are primarily saline, but some fresh water aquifers occur at depths of more than 2000 m [*Thomas*, 2000]. The fluid flux and the relatively low temperature in the subsurface strata make this region suitable for microbial life, and our hypothesis is that microorganisms inhabit (or did inhabit) the subsurface volcanic rocks at this site.

2. Samples and Methods

2.1. Samples

[9] HSDP cores were archived dry and at room temperature at the California Institute of Technology and are now at the American Museum of Natural

History. Polished, petrographic thin sections representative of most lithologic units were made by the drilling program. We examined archived and new thin sections from subaerial basalt lava flows (surface to 1080 m) and from the deeper (>1080 m) basalt hyaloclastites. Some of the lava flows had small amounts of fresh glass (Figure 2a), and voids and fractures in the glass were surrounded by alteration zones from which short, blunt, rounded buds extend into the glass (Figure 2b). This style of alteration of glass is quite distinct from the alteration found in the glassy margins of deep sea pillow basalts which has been associated with microorganisms. The blunt, rounded buds in the lava flows may be mediated by microbial activity, but because of the small amount of glass in the flows compared to the deeper hyaloclastites, we focused our effort on the hyaloclastites.

[10] The glass shards in hyaloclastites are partially or completely altered to smectite clay and palagonite [*Walton and Schiffman*, 2003]. Where unaltered glass fragments remain, some have tubes that extend into the glass [*Fisk et al.*, 2001; *Walton and Schiffman*, 2003], and the tubes appear similar to the alteration of deep sea basalt glass that has been attributed to microorganisms [*Fisk et al.*, 1998; *Furnes et al.*, 2001]. The deep hyaloclastites (>1800 m) mostly have sharp boundaries between glass and secondary minerals (on the basis of microscopic examination at up to 400x magnification, Figures 2c and 2d), and these sharp boundaries suggest that the alteration is abiotic.

[11] Shallow hyaloclastites have closely spaced tubes that are 1 to 3 μm in diameter and that penetrate glass shards from the altered surface (Figures 2e–2h). This style of alteration has been previously attributed to the activity of microorganisms. For example, in thin section R619-3.5 (Figures 2e and 2f) from a hyaloclastite unit at 1570 m below the surface the alteration is similar to that displayed in Figure 4C of *Furnes et al.* [2001], Figure 1D of *Furnes and Staudigel* [1999], and Figure 1G of *Fisk et al.* [1998]. Another thick deposit of hyaloclastite (Unit 198, 1336 m to 1404 m which is composed primarily of olivine basalt glass that is cemented with reddish-brown secondary minerals) has abundant tubes that also suggest

microbial activity (Figures 2g and 2h). Because many of the glass shards in Unit 198 appeared to be modified by microbial activity, and because Unit 198 is relatively thick and therefore provided a large amount of material with which to work, we applied most of our further investigation to the samples from this unit. Within this interval R530-9.8, R530-10.1, and R543-7.8 indicate bulk samples of the core and R531-9.3 is a petrographic thin section (Figure 1g).

[12] Sample R530-10.1 was a 6-cm-long piece of core which was split in an enclosed clean bench with a single strike with a sterile chisel and hammer. Pieces from the center of the core were selected with flamed tweezers and placed in clean vials until they were examined by UV laser induced fluorescence (LINF) imaging, UV resonance Raman (UVRR) spectroscopy, and environmental scanning electron microscopy (ESEM) with energy dispersive X-ray spectrometer. Another piece of Unit 198 (R530-9.8) was also subsampled under sterile conditions and analyzed for amino acids and nucleic acids.

2.2. Methods

2.2.1. Thin Section Analysis

2.2.1.1. Electron Microprobe

[13] Quantitative, twelve-element, electron microprobe analyses (Table 1) were acquired with a four-spectrometer CAMECA SX-50 at Oregon State University. Analyses of glass and alteration products were made with an accelerating voltage of 15 kV and a beam current of 10 nA. Element peak intensities were counted for 10 s except F, Ti, and Fe, which were counted for 20 s. Backgrounds on each side of the peak location were counted half as long as the peak. Well characterized mineral and glass standards were used for calibration and internal standards.

2.2.1.2. Staining/Epifluorescence

[14] Acridine orange (AO) binds to RNA and to both single and double stranded DNA, and it absorbs light of wavelength 440 to 480 nm [*Kemp et al.*, 1993]. AO bound to double stranded DNA produces green fluorescence (520 nm), and AO
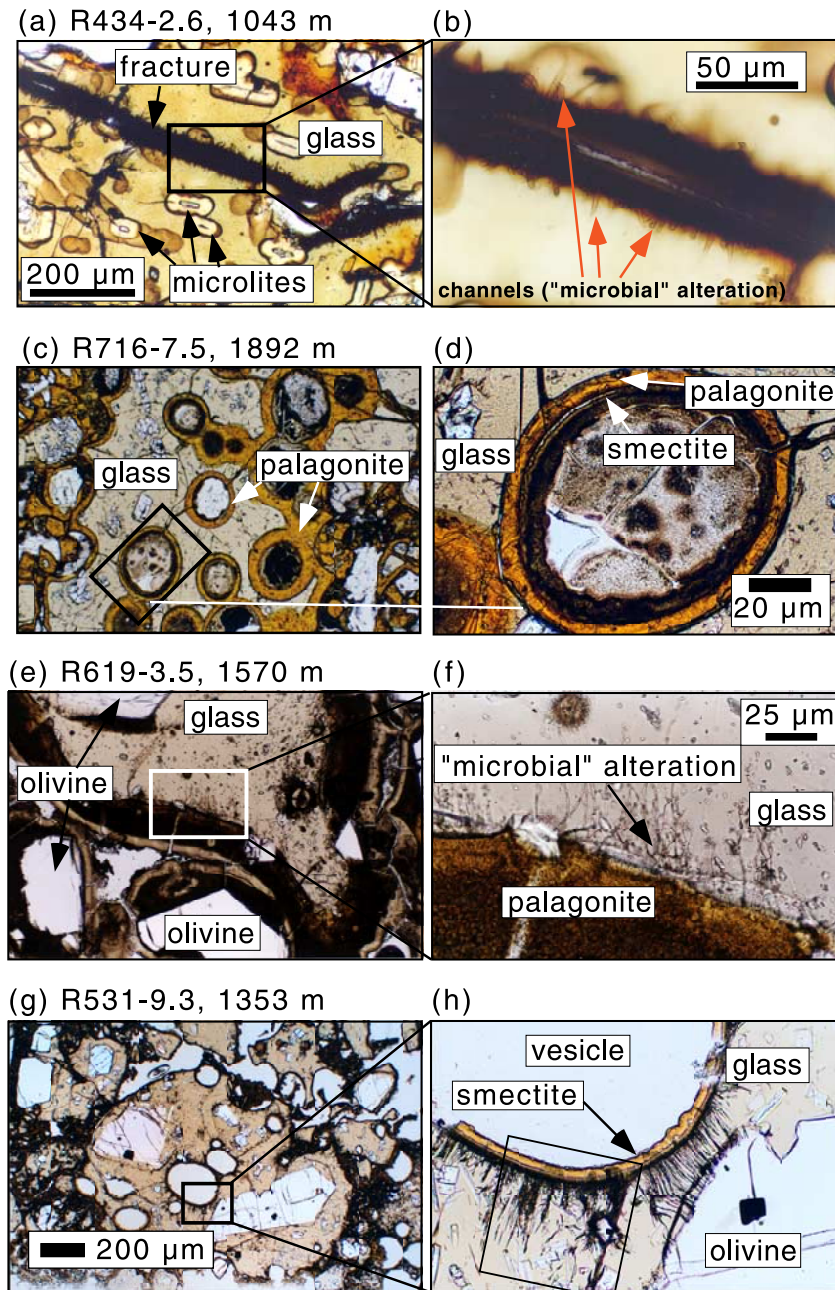
Figure 2. Photomicrographs in plane polarized light of fresh and altered glass from the Hawaii Scientific Drilling Program site. (a) Fresh and altered glass of HSDP R434-2.6 from subaerially erupted lavas. Seawater is present at this depth in the hole. Tan glass contains microlites surrounded by light alteration zones. The dark zone through the center of the photo is surrounded by tubes which are shown in detail in b. (b) Dark zone is centered on an open fracture or collapsed vesicle. Tubes are about 10 μm long and 4 μm in diameter. (c and d) Fresh and altered glass from hyaloclastite R716-17.5 from 1892 m. Glass shards are surrounded by clay and vesicles are rimmed by palagonite and smectite. The boundaries between glass and palagonite are smooth and do not contain the "microbial" tubes seen in shallower levels of the hole. (e and f) Fresh and altered glass from hyaloclastite R619-3 from 1570 m. Glass fragments and olivine are surrounded by smectite clay. "Microbial" alteration of the glass is in the form of fine (1 μm diameter) tubes that penetrate the glass. The glass of R619-3.5 does not have the red oxidative alteration of R434-2.6. (g and h) Photomicrographs of Unit 198 sample R531-9.3 from 1353 m below sea level. (g) Olivine up to 500 μm and round and ovoid vesicles up to 200 μm are present. Rectangle shows location of h. (h) Vesicle rimmed with 10 μm thick layer of yellow smectite, an opaque zone, and dark tubes that extend into glass and up to olivine. Box is area of elemental X-ray scan (Figure 3).

Table 1. Electron Microprobe Analyses of Glass and Vesicle Filling From HSDP 531-5.9 and 779-9.8

	Oxide wt.%											
	SiO_2	TiO_2	Al_2O_3	FeO	MnO	MgO	CaO	Na_2O	K_2O	P_2O_5	Cl	F	Sum
	HSDP 531-5.9 (1353 m)											
1 fresh glass	49.29	3.19	13.59	12.28	0.16	6.65	11.15	2.53	0.51	0.28	0.02	0.24	99.91
2 altered glass at edge of vesicle	44.97	2.93	12.50	11.41	0.17	6.15	10.30	2.27	0.48	0.29	0.02	0.18	91.68
3 smectite next to glass	46.97	1.17	9.20	7.68	0.12	15.01	2.57	1.19	0.60	0.34	0.22	1.03	86.11
4 smectite next to void	51.89	0.12	9.90	7.15	0.08	18.49	1.70	0.94	0.75	0.00	0.23	1.07	92.31
	HSDP 779-9.8 (2226 m)											
5 fresh glass	52.37	2.71	13.51	10.55	0.22	6.86	10.79	2.39	0.41	0.29	0.00	0.19	100.07
6 altered glass	51.00	3.39	13.57	9.62	0.10	5.18	11.31	1.89	0.34	0.19	0.30	0.11	96.60
7 gel palagonite	44.99	4.80	12.45	6.45	0.01	1.19	12.83	1.05	0.16	0.16	0.84	0.00	84.09
8 fibropalagonite	48.32	0.37	11.52	11.67	0.17	10.97	6.28	0.21	0.13	0.00	0.57	0.12	89.64
9 fibropalagonite	46.43	0.24	9.64	11.60	0.22	12.91	5.02	0.38	0.09	0.01	0.35	0.18	86.55

bound to RNA or single stranded DNA has an orange-red fluorescence (650 nm [*Shapiro*, 1988; *Romeis*, 1968; *Stockert and Lisanti*, 1972]). Thus structures containing double stranded DNA (e.g., cell nuclei, chromosomes and viral inclusions) fluoresce green to yellow-green, and structures containing RNA (e.g., ribosomes, nucleoli and viral inclusions) and single stranded DNA fluoresce red. More active cells (with more rRNA) are orange to red while dormant cells (more DNA) are more yellow-green.

[15] Petrographic thin sections were submerged in filter sterilized solution (0.2 μm pore size) of 0.1% AO dissolved in phosphate buffered saline solution (PBS buffer [*Sambrook et al.*, 1989]) and then subjected to a partial vacuum until degassing became visible. The overall incubation time with the dye was 15 minutes after which the sample was washed with 200 to 300 ml of filter sterilized PBS buffer. During washing the sample was cycled to partial vacuum and back to atmospheric pressure to draw stain out of surface cracks and pits.

2.2.2. Interior Core Analyses

2.2.2.1. UV Laser-Induced Native Fluorescence (LINF)

[16] Visible light and fluorescent images of a freshly cleaved sample were acquired at 60X, 300X, or 800X magnification. The same sample was excited at 224.3 and 248.6 nm using a helium charge exchange pumped sputtering silver or copper hollow cathode laser (Photon Systems, Model HeAg60-224SL and Model NeCu60-248SL, respectively). The lasers require no pre-heating and operate in a chopped-continuous wave fashion at 1% duty cycle to minimize sample heating effects. The laser produced a spot 40 μm in diameter at 800X.

[17] Images were recorded using a cooled CCD camera employing a SONY ICX085AL Interline Transfer CCD, 16.9 μm wide, and containing $1300 \times 1030 \times 6.7 \ \mu m^2$. Average power delivered to samples was 20 μW for the 224.3 nm laser and 100 μW at 248.6 nm excitation. Visible light reflectance images were obtained with ~100 ms exposure time. UV native fluorescent image exposures were acquired in ~30 seconds at 248.6 nm and ~60 seconds at 224.3 nm. Because of the 1% duty cycle, this means total UV exposure time was 0.5 and 1.0 s, respectively. The technique is sensitive enough to detect a single 1 micrometer microorganism against a basalt, plagioclase, or calcite background.

2.2.2.2. Deep Ultraviolet Resonance Raman (UVRR) Spectroscopy

[18] After using the UV-LINF to determine the location of organic compounds in the sample, Raman spectra were acquired using a 0.55 m, f/6.4 fully automated Czerny-Turner imaging spectrograph (Instruments SA, TR550MST1) with 1800 g/mm low stray light holographic. The CCD detector assembly uses a 2048×512 array of

13.5 μm square pixels back illuminated and UV antireflection coated detector (English Electric Valve) temperature regulated and mounted in a liquid nitrogen cooled dewar.

[19] Raman spectra were obtained with 248.6 nm laser excitation at 800X magnification with a spot size of ~40 μm and a collection time of 60 s. Actual UV excitation time of 600 ms spread over the 60 s, and average power delivered to the sample of less than 10 μwatts minimized sample heating and saturation effects.

2.2.2.3. Environmental Scanning Electron Microscopy (ESEM)

[20] A Philips XL30 ESEM with a field emission gun was used to view hydrated, uncoated samples of the freshly exposed surfaces of HSDP sample R530-10.1. The field emission gun on the ESEM allows high resolution imaging with a beam diameter at the specimen of approximately 10 nm in "wet" mode (5.4 Torr water vapor pressure in this case). Conditions for the images presented here were 20 kV, magnification of 2,500X to 6,500X, and working distance of 10.6 mm. Visible reflectance images were used to guide the electron microscope imaging.

[21] Morphological features were probed with energy dispersive X-ray spectroscopy to provide elemental composition and possible identification of features as biological or geological.

2.2.3. Bulk Core Analyses

2.2.3.1. Amino Acid Analysis

[22] Sample R543-7.8 is a few meters from sample R530-10.1 yet still within Unit 198. The basalt was split open and an interior sample of approximately 17 g isolated. This interior sample was crushed and then extracted with 6N double distilled HCl at 100°C for 12–16 hr. The extract was desalted using AG50W-X8 cation exchange resin prior to amino acid analysis. Amino acid analyses were carried out by high pressure liquid chromatography (HPLC) separation of fluorescent diastereomeric derivatives [*McDonald and Bada*, 1995; *Zhao and Bada*, 1995]. Desalted extracts were derivatized with o-phthaldialdehyde/N-acetyl-L-cysteine, and

the derivatives separated and identified by reverse-phase HPLC using a C18 column (Phenomenex) with 50 mM sodium acetate and methanol as the solvent system. Eluting amino acid derivatives were detected using a fluorescence detector, with excitation λ_{ex} = 340 nm and emission λ_{em} = 450 nm. Duplicate HPLC runs were carried out on the extract, and amino acid standards were used to calibrate retention times and detector response. A sample of crushed Suprasil quartz previously combusted at 500°C for 2 hr was used as a procedure blank, and the background amino acid concentrations from this blank were subtracted from those detected in the basalt sample.

2.2.3.2. DNA Extraction and Amplification

[23] The inner portion of core sample R530-9.8 was obtained using sterile techniques and powdered with a DNA-free tungsten mortar and pestle (baked at 220°C for 24 hours). A small volume (2 ml) of rock powder was used in each of two extractions. Two control DNA extractions in which no rock material was added were performed to detect contamination introduced during sample handling or from the DNA extraction reagents.

[24] To each extraction tube (per 2 ml rock powder) the following were added: 2.5 ml TE pH 7.4, 1.0 ml 25% Chelex-100 (w/v), 1.53 ml 0.5M EDTA, pH 8.0, 380 μl 10% SDS (w/v), 100 μl proteinase K (20 mg/ml, Qiagen Inc., Valencia, CA). Tubes were placed in a 37°C rotator with gentle agitation (180 rpm) overnight. The rock powder was separated from the supernatant through low speed centrifugation and the following ingredients (per ml of supernatant) were added: 166.7 μl 5M NaCl and 133.33 μl 10% CTAB/0.7M NaCl solution. Samples were incubated at 65°C for 30 minutes, extracted once with phenol/chloroform/isoamyl alcohol (25:24:1), pH 7.4, and then extracted twice with chloroform/isoamyl alcohol (24:1). The DNA was precipitated by adding one volume of isopropanol and incubating the samples overnight at 4°C. The samples were spun at 20,000 rpm for 60 minutes at 4°C in an ultracentrifuge (Beckman Instruments, Inc., Palo Alto, CA) to pellet the precipitated DNA. Pellets were washed with 70% ethanol and dried in a laminar flow hood

at room temperature. The dried DNA was suspended in 40 μl sterile water and stored at −80°C.

[25] Domain-specific primers were used to amplify the 16S rRNA genes from the archaeal and bacterial communities, respectively. The archaea-specific primers Arch20F 5′-TTC CGG TTG ATC CYG CCR G-3′ [*DeLong et al.*, 1999] and Arch915R 5′-GTG CTC CCC CGC CAA TTC CT-3′ [*Stahl and Amann*, 1991] were used to amplify the archaeal community. For the bacterial community, the bacterial-specific primers 27F-B 5′-AGA GTT TGA TCM TGG CTC AG-3′ and 1492RY 5′-GGY TAC CTT GTT ACG ACT T-3′ were used. PCR reactions (25 μl volume) contained final concentrations of the following: 1 μl of DNA extract; 1% (v/v) PCR buffer (MBI Fermentas + NH$_4$SO$_4$); 0.2 mM each deoxynucleotide triphosphate; 0.2 μM each primer; 2 mM MgCl$_2$ (MBI Fermentas); 1.2 mg/ml bovine serum albumin (non-acetylated, SIGMA cat# A-7906); 0.25 U Taq polymerase (MBI Fermentas). Cycling conditions were 50 cycles of denaturation at 94°C for 1 min, annealing at 55°C for 1 min, and extension at 72°C for 2 min. Amplification products were cleaned with the QIAquick PCR Purification Kit (Qiagen Inc., Valencia, CA) and cloned into the pGEM®-T Easy vector (Promega Corp., Madison, WI). A clone library was constructed and screened according to the methods of *Vergin et al.* [2001]. According to this approach, restriction enzyme analysis with two four-cutter enzymes was used to separate the clones into distinct clone families.

2.2.3.3. Phylogenetic Analysis

[26] Twelve clones were sequenced with the ABI Big-Dye sequencing chemistry according to the manufacturer's instructions (Applied Biosystems, Inc. [ABI], Foster City, CA). Sequences were assembled using the ABI Autoassembler program (ABI) and aligned to other 16S rDNA sequences using BioEdit version 5.6.0 [*Hall*, 2000]. A neighbor-joining tree was obtained on the basis of 610 bp of unambiguously aligned sequence using the Kimura 2-parameter distance method [*Kimura*, 1980] in PAUP* version 4.0 b10 [*Swofford*, 2001]. The 16S rDNA sequences for the twelve clones have been submitted to the GenBank database and

have been assigned accession numbers AY267806 to AY267817.

2.3. Contamination During Sample Collection, Storage, and Preparation

[27] Microorganisms were certainly introduced into the HSDP hole with water and drilling mud that were used in the drilling process. However, no attempt was made to quantify the contamination. Additional organisms could have been introduced into samples during sample processing and storage. In this study we used a number of techniques to detect signals that could arise from organisms in the rocks. Some of these signals are likely to have been present before the rocks were drilled and some could have been introduced during or after drilling. In the Discussion section we evaluate which data are most likely to indicate presence of life in the rocks before drilling and which signals could have been the result of contamination.

3. Results

3.1. Electron Microprobe

[28] Representative analyses of glass, palagonite, and clay for two depths in the hole are given in Table 1. These analyses are from evenly spaced, 5-μm-diameter, spot analyses starting in the fresh glass and progressing into altered glass and then into palagonite or clay. HSDP 531-5.9 (1353 m) is a sample with abundant physical evidence of microbial activity, and HSDP 779-9.8 (2226 m) has minor evidence of microbes. The two fresh glass analyses (#1 and #5 in Table 1) are typical of Hawaiian olivine basalts (E. Stolper et al., Glass in the submarine section of the HSDP2 drill core, Hilo, Hawaii, submitted to *Geochemistry, Geophysics, Geosystems*, 2003). The smectite clay lining vesicles at 1353 m (see yellow lining of vesicle in Figure 2h; Table 1, analyses #3 and #4) is similar to that described by *Walton and Schiffman* [2003]. An orange alteration of the rim of the vesicle at 2226 m is isotropic palagonite (gel palagonite) which is similar to the orange vesicle lining in Figure 2d. This phase is notably enriched in TiO$_2$, CaO, and Cl and depleted in MgO (Table 1, analysis #7) compared to smectite at
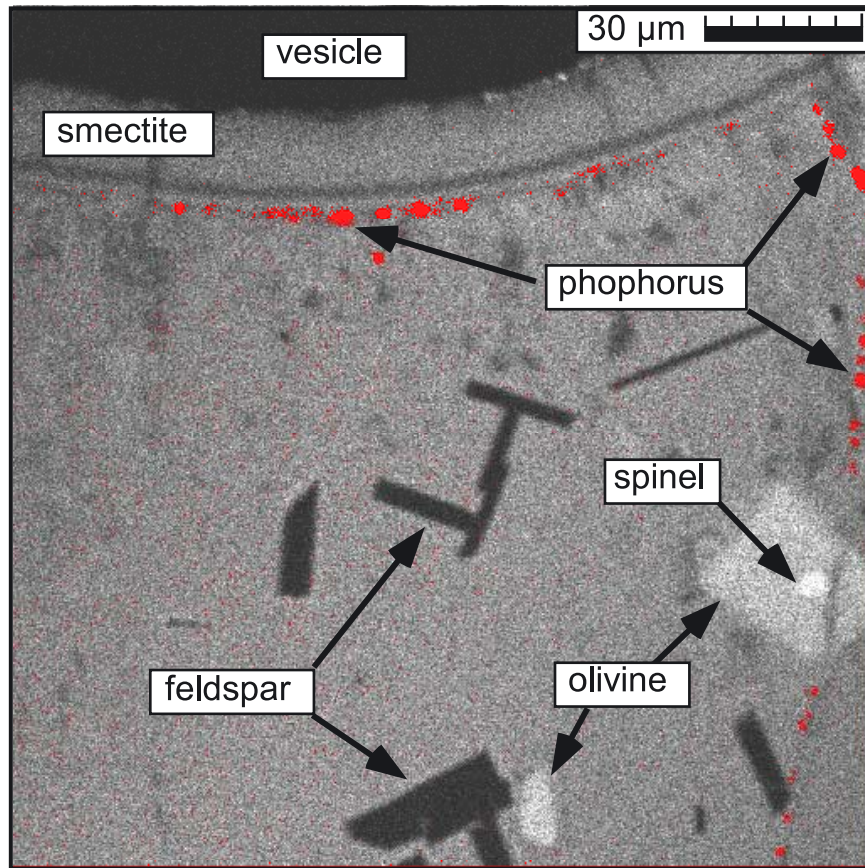
Figure 3. Electron microprobe elemental map of iron and phosphorus in sample R531-9.3. See box in Figure 2h for the location of the image in the sample. Clay and glass are a similar intensity and have similar amounts of Fe (10 ± 3 wt.% FeO). Olivine with approximately 15 wt.% FeO and spinel with 20% FeO appear lighter than the glass. Dark angular areas are feldspars which have less than 1% FeO. Open space in the vesicle (top of image) is also black. The location of phosphorus is highlighted by the red overlay. Phosphorus is concentrated in regions each about 5 μm in diameter and separated by about 10 μm. On the right side of the image phosphorus is concentrated along a fracture except where the fracture crosses a grain of olivine.

1353 m. The dark interior lining of the vesicle adjacent to the gel palagonite is fibropalagonite (Table 1, analysis #8 and #9).

[29] The microprobe was also used to acquire 200 μm by 200 μm elemental maps. One of these maps of the area indicated by the box in Figure 2h is shown in Figure 3. In this image the spectrometers were optimized for Fe and P Kα X-rays. The Fe map is useful for showing the mineral phases, voids, and the location of elements associated with life [*Torsvik et al.*, 1998]. For example, the void inside the vesicle (top of image) and angular feldspars appear black indicating no Fe signal. Glass and smectite are a similar gray due to 10 ± 3 wt.% FeO. An olivine and its spinel inclusion have the highest iron (>15 wt.% FeO) and are the lightest gray. The X-ray signal from P is superimposed on the Fe X-ray map to show the location of phosphorus relative to the vesicle rim and mineral phases. Phosphorus is present in 5 to 10 μm diameter patches in the altered margin of the glass and along a fracture extending into the glass (right side of image). In the patches P_2O_5 concentrations are 50% to 100% above the background in the glass (0.28 wt.% P_2O_5).

3.2. Staining/Epifluorescence

[30] Figure 4 is a petrographic thin section of sample HSDP 531-5.9 from 1353 m below sea level viewed in the epifluorescence microscope.

Figure 4a is a transmission visible light view of the rim of a vesicle revealing smectite clay, glass, and a region of tubes that penetrate into glass. This brightfield illumination through a 30 μm thick petrographic section results in lower resolution than in Figure 2; however, the shapes and sizes of the features are the same as those shown in Figures 2g and 2h. Figure 4b is the epifluorescence image of the vesicle rim after staining with acridine orange. Nonspecific binding of acridine orange (yellow to green) occurs in the smectite lining the vesicle. However, heterogeneous staining enhancement occurs in bands within the smectite and within the tubes projecting into the glass. This fluorescence is intense, variable in color, and occurs as a mixture of individual coccoid shapes and as chains, a pattern suggestive of microbial cells.

3.3. UV Laser Induced Native Fluorescence (LINF) and Resonance Raman Spectroscopy

[31] Visible light photomicrographs and UV excited fluorescence of HSDP 530 10.1 in Figure 5 reveal a remarkable distribution for LINF activity. Figure 5a is a 60X magnification of the sample using broadband visible light for illumination. Broken vesicles are apparent as ≤300 μm diameter hollow spheroids. Figures 5b and 5d are visible light images at increasing magnification of the areas outlined by the boxes. Figures 5c and 5e are the respective matching LINF images of the area shown to the left of each image. Maximum LINF activity is found along the vesicle rims and at isolated locations within the glass. Samples of olivine separated from R530-10.1 showed no LINF activity for 224.3 and 248.6 nm excitation.

[32] Figure 6 illustrates a Raman spectrum from a region of clay that exhibited laser induced fluorescence (Figure 5e) and which lined the interior of a vesicle. The spectrum reveals activity between 1300 and 1600 wave numbers (cm^{-1}) expected from vibrational bending and stretching of heterocyclic and homocyclic ring structures [*Perno et al.*, 1989; *Manoharan et al.*, 1990; *Asher et al.*, 1991]. Such resonance activity is usually associated with the presence of nucleic acids and aromatic amino

acids [*Nelson et al.*, 1992]. The strong peak at 470 cm^{-1} can be assigned to silica, the activity at 800 cm^{-1} is most likely the barely resolved doublet of olivine, and the peak at 1086 cm^{-1} is characteristic of calcite [*Wang et al.*, 1995, 1999]. The Raman activity at 949 cm^{-1} is most similar to the calcium phosphate signature found in the varnish coatings of basalt cobbles from the Lunar Crater volcanic field in Nevada [*Israel et al.*, 1997]. The broad region of activity around 3300 cm^{-1} can be assigned to water.

3.4. Environmental Scanning Electron Microscopy

[33] Figure 7a is an ESEM image (acquired at 2,500X) of smectite clay lining a fractured vesicle and of the fractured glass surface outside the vesicle. The boxes show the areas depicted in Figures 7b and 7c. Figure 7b was acquired at 5,000X and shows pitted glass and two clay-covered spheroids (center and lower left). Figure 7c (6,500X) shows one cell cluster along the edge of the vesicle. The location and size of the cluster are similar to those of phosphorus concentrations identified with the electron microprobe and depicted in Figure 3. ESEM elemental analyses confirmed the presence of carbon and phosphorus in the cell clusters.

3.5. Amino Acid Analysis

[34] The concentrations of amino acids detected in the sample in moles per gram of rock are shown in Table 2. Four amino acids, serine, glycine, alanine, and valine, were detected. Tryptophan and proline are not detectable with the methods used. All other protein amino acids were below detection limits (approximately 10^{-12} mol amino acid per gram rock). These concentrations are comparable in magnitude to those found in the deep interior of Antarctic dry valley sandstones [*Sun et al.*, 2000] and in Martian meteorites [*McDonald and Bada*, 1995; *Bada et al.*, 1998; *Glavin et al.*, 1999].

3.6. PCR Amplification and Cloning of Prokaryotic 16S rDNA

[35] Although no amplification of bacterial 16S rRNA genes was detected after 50 cycles of PCR, archaeal 16S rDNA was readily detected with the
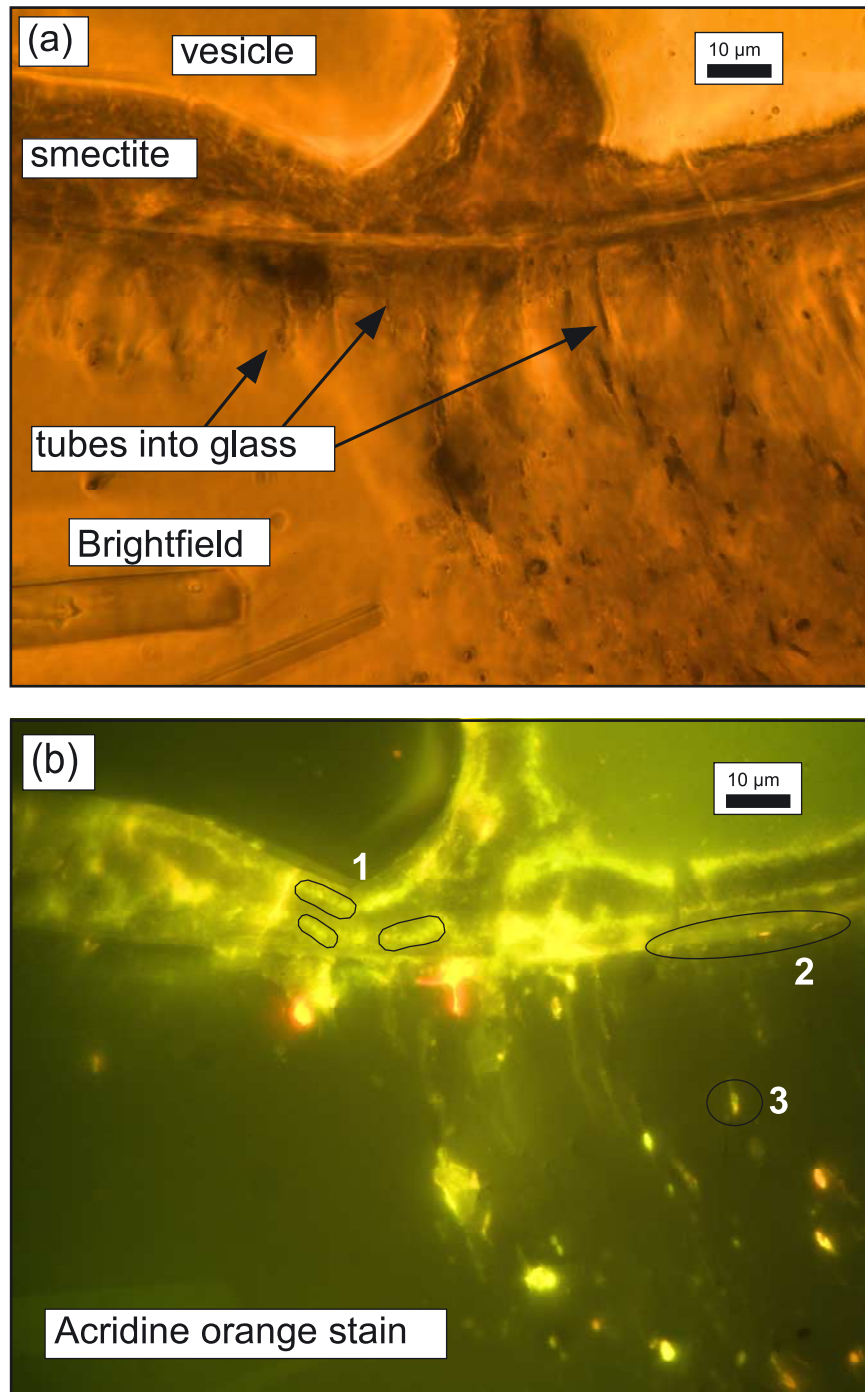
Figure 4. Petrographic thin section of sample HSDP 531-5.9 from 1353 m below sea level viewed in the epifluorescence microscope. (a) Brightfield illumination of the rim of a vesicle. Smectite clay, glass, and region of tubes into glass can be distinguished. (b) Fluorescence image of the same region as in (a) after staining with acridine orange. The most intense fluorescence is along the margin of glass and smectite where the density of tubes is greatest. Heterogeneous staining occurs within tubes into the glass and in regions in the smectite. The size, shape, and distribution of fluorescence within smectite suggest the presence of microorganisms (three encircled areas labeled 1). Both red and green fluorescence are present at the smectite-clay margin (area 2). Granular red and green fluorescence occurs where a tube is exposed at the surface of the thin section (area 3).
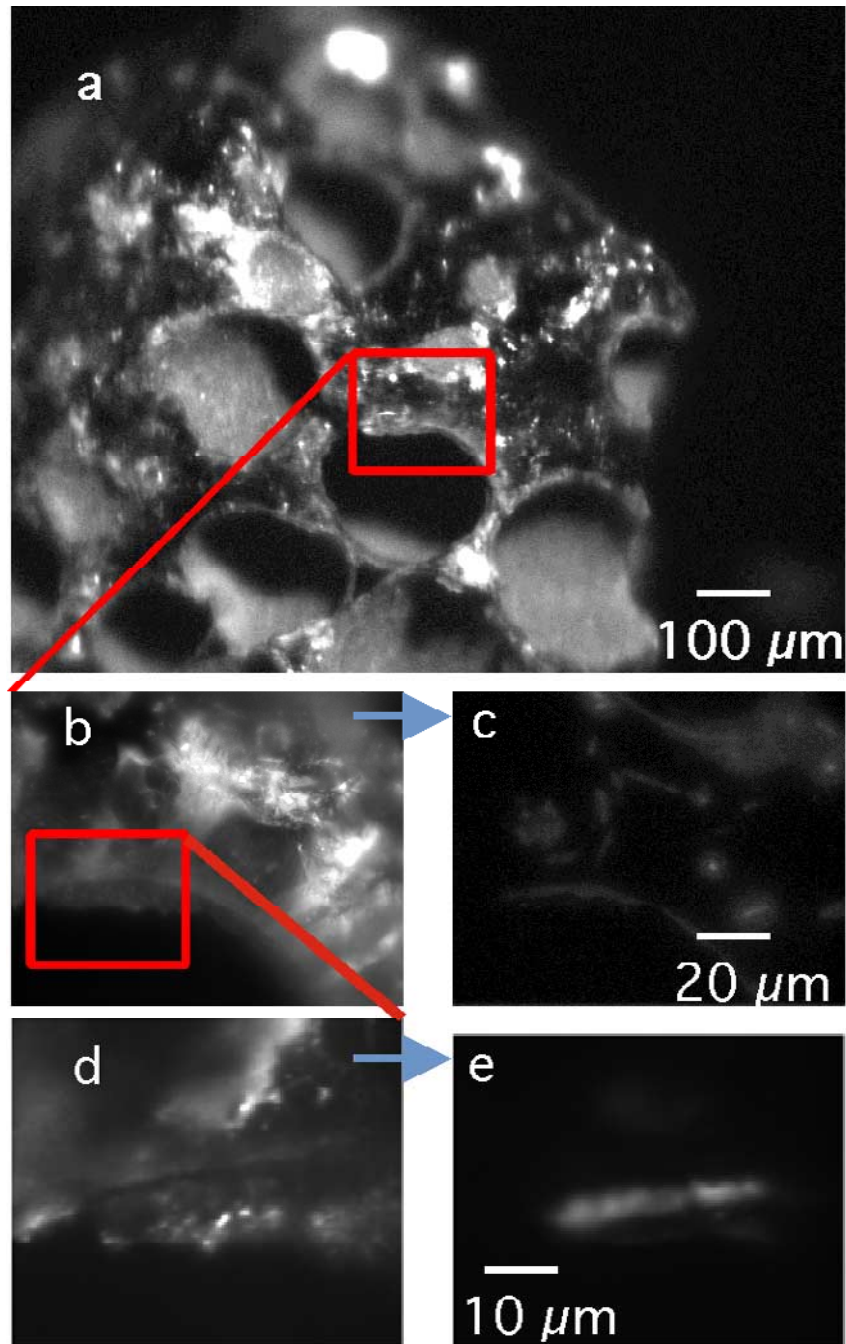
Figure 5. Incident light photomicrographs and 224 nm UV excited native fluorescence of HSDP 531-10.1. (a) Glass contains vesicles (gas bubbles) up to 300 μm in diameter. (b and d) Incident light images of the areas outlined by the boxes. (c and e) Fluorescence signals from the areas shown in the b and d, respectively. In c fluorescence is seen in the clay rim of the vesicle and at isolated locations in the glass. In e the fluorescence is found 2 to 5 μm inside the clay that lines the vesicle.

Geochemistry
Geophysics
Geosystems

G^3

FISK ET AL.: HAWAIIAN SUBSURFACE BASALTS
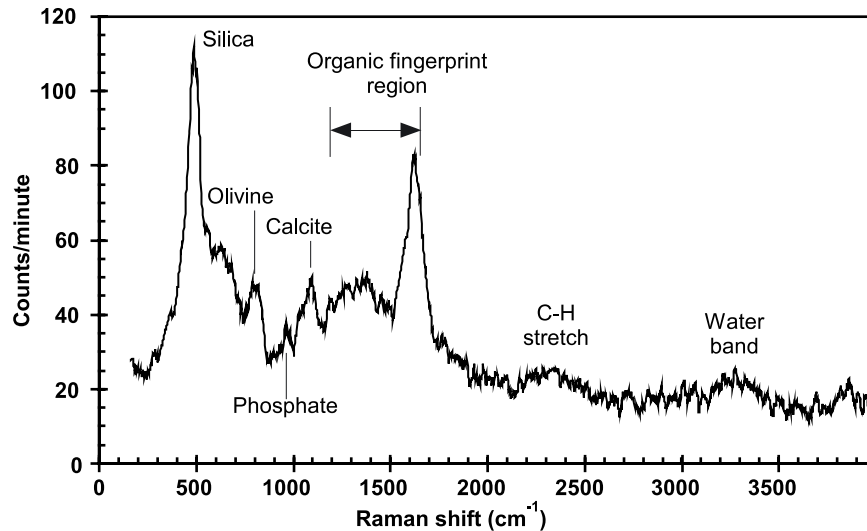
10.1029/2002GC000387

Figure 6. Resonance Raman data were obtained with 248.3 nm laser excitation of the sample area shown in Figures 4d and 4e. The activity between 1200 and 1600 wave numbers (cm^{-1}) is expected from vibrational bending and stretching of heterocyclic and homocyclic ring structures of nucleic and aromatic amino acids (see text for details). The strong peak at 470 cm^{-1} can be assigned to silica, the activity at 800 cm^{-1} is most likely the barely resolved doublet of olivine, and the peak at 1086 cm^{-1} us characteristic of calcite. The Raman activity at 949 cm^{-1} is most similar to the calcium phosphate signatures found in the varnish coatings of basalt cobbles from the Lunar Crater volcanic field in Nevada [*Israel et al.*, 1997]. The broad regions of activity around 2300 cm^{-1} and 3300 cm^{-1} result from −CH and water, respectively.

same cycling parameters. After further PCR attempts using a variety of bacterial primer combinations with no success, we decided to clone and describe only the archaeal community. A 92-member clone library of the archaeal community 16S rDNA was constructed and screened with restriction analysis. Based upon restriction fragment length polymorphism (RFLP) analysis using two restriction endonucleases (HaeIII and MboI) 77 of the 92 clones belonged to seven different clone families containing three or more clones, while 15 of the clones were unique. Twelve clones representing each of the seven most abundant clone families as well as five additional unique clones were sequenced for identification. BLAST (Basic Local Alignment Search Tool) searches [*Altschul et al.*, 1990] of the National Center for Biotechnology Information sequence database (GenBank) were performed to determine rough identities of the unknown clone sequences. Eleven of the clones were 97 to 99% similar to uncultured Group I marine Crenarchaeotes previously identified from various hydrothermal vent, subseafloor, and deep ocean trench habitats, while one of the clones was

95% similar to a Group II Euryarchaeon, clone SBAR1A (GenBank accession no. M88074).

[36] A phylogenetic tree (Figure 8) depicting the relatedness of the Hawaiian drill core clones from this study (indicated in blue) with close relatives from the GenBank database was constructed with phylogenetic analysis software (PAUP* beta version 4.10 [*Swofford*, 2001]) by neighbor joining analysis using the Kimura 2-parameter distance method. From this analysis, two major groups within Group I Crenarchaeota emerged. Eight of the Hawaiian drill core clones clustered with Crenarchaea identified from hydrothermal vent [*Moyer et al.*, 1998] or mid-ocean ridge subseafloor [*Huber et al.*, 2002] habitats with presumably warmer in situ temperatures than the HSDP hole (Figure 8). Three clones clustered with Crenarchaea identified from colder, deep ocean sediment habitats such as the Mariana trench [*Kato et al.*, 1997] and Japan Trench [*Li et al.*, 1999]. Hawaiian drill core clone HD7 clustered with a Group II Euryarchaeote identified from the water column of Santa Barbara channel [*Massana et al.*, 1997]. This Group II
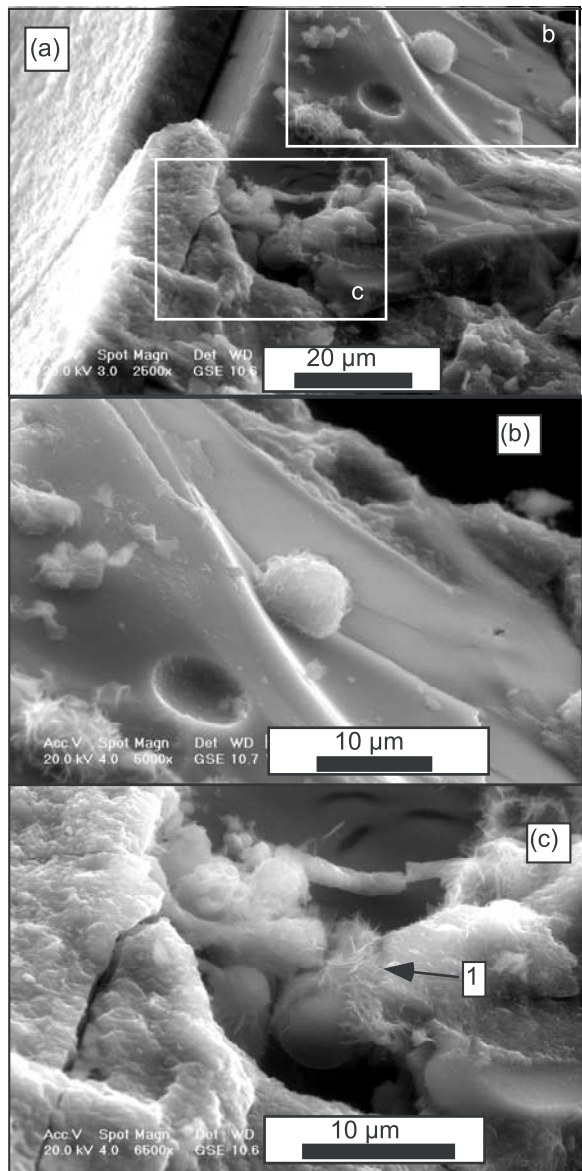
Figure 7. Environmental scanning electron microscope images of the rim of a vesicle in R530-10.1. (a) Image at 2,500X. Boxes show areas of lower images. Margin of vesicle showing smectite on the left and the interior of the vesicle. The smectite layer is about 10 to 15 μm thick at this location. To the right of the clay in the upper part of the image is smooth glass and what appear to be mineralized cells in box b. (b) Two 5-μm diameter, clay covered spheroids and a pit in glass of the same size. (c) 6,500X image of clay and cell-like objects at the margin of the vesicle. These objects are about 5 μm from the smectite-glass boundary which is similar to the depth within the glass of regions of intense fluorescence due to staining with acridine orange (Figure 4). The size and distribution of cell clusters are similar to the distribution of P along the edges of vesicles (Figure 3). ESEM elemental analysis confirmed carbon and phosphorus in the cell clusters.

Euryarchaeote could have been introduced into the basalt as a result of using a mixture of seawater and drilling mud during coring.

4. Discussion

4.1. Clay and Palagonite

[37] Secondary minerals in upper 300 m of HSDP hyaloclastites are dominantly smectite clay with minor palagonite [*Walton and Schiffman*, 2003], and with increasing depth in the core additional phases of smectite and palagonite alteration are present as well as zeolites. The unit we examined in detail (Figures 2g and 2h) was within the upper 300 m of the hyaloclastites and was in an area of extensive tube formation in glass. The composition of the smectite rim of the vesicles next to the tubes (Table 1, analyses #3 and #4) is similar to the smectites reported previously for the shallow hyaloclastites [*Walton and Schiffman*, 2003]. Deeper in the hole palagonite rather than smectite is adjacent to the glass that contains tubes (Figure 2f) and in some samples palagonite occurs next to glass that has no tubes (Figure 2d). The palagonite has lower Mg, K, and F, and higher Ti and Ca than the smectite. Where palagonite is associated with tubes in glass, its Fe content is 50% to 100% higher than palagonite that is not associated with tubes, otherwise the two occurrences of palagonite have similar compositions.

[38] The reason for the association of what we interpret as microbial activity (tubes) with smectite and why tubes are absent or in low abundance deep in the hole is not known. One possible explanation is that the physical or chemical conditions in the deeper (and warmer and older) parts of the hole inhibit the growth of microorganism and promote the formation of palagonite. This could happen at depth because much of the pore space has been filled with zeolites (compare Figures 2c and 2d with Figures 2g and 2h) which could reduce fluid flow through the formation. In the shallow hyaloclastites high porosity would allow high fluid flux (a hypothesis that is supported by the depressed thermal gradient down to 1500 m) which could sustain microbes growing on the surfaces of glass shards. Whether microorganisms influence the

Table 2. Amino Acid Analysis of Sample R543-7.80

Amino Acid	Total Moles		Corrected Moles		
	Blank[a]	Sample[a]	Sample[a]	Moles/g Rock[a]	Std. Dev.
L-Serine	8.2×10^{-10}	9.1×10^{-10}	9.4×10^{-11}	5.5×10^{-12}	7.0×10^{-12}
Glycine	2.1×10^{-9}	2.5×10^{-9}	4.5×10^{-10}	2.6×10^{-11}	6.1×10^{-12}
D-Alanine	2.0×10^{-10}	2.7×10^{-10}	6.5×10^{-11}	3.8×10^{-12}	2.7×10^{-12}
L-Alanine	7.1×10^{-10}	1.4×10^{-9}	6.7×10^{-10}	3.9×10^{-11}	1.5×10^{-11}
L-Valine	6.8×10^{-10}	1.9×10^{-9}	1.2×10^{-9}	6.8×10^{-11}	4.2×10^{-11}
Total amino acids detected				1.4×10^{-10}	

[a] Average of three analyses.

mineralogy or chemistry of the glass alteration products is still not known. The higher FeO (13 to 14 wt.%) in palagonite adjacent to glass with tubes (Figure 2f) compared to FeO of 9 to 10 wt.% in palagonite adjacent to glass without tubes (Figure 2d) may be an indication of microbial influence on palagonite composition. The closely spaced tubes on the rims of vesicles where only smectite is present may indicate chemical transport through the clay may support microorganisms. On the other hand, the low abundance or absence of tubes where palagonite is present may indicate that palagonite limits the transport of metabolic substrates from fluids to the glass and inhibits microbial activity at the interface of glass and palagonite.

4.2. Stained Nucleic Acids

[39] Several dyes specific for nucleic acids bind to regions of igneous rocks that have tubes like those shown in Figures 2f and 2h [*Thorseth et al.*, 1995; *Furnes et al.*, 1996, 2001; *Giovannoni et al.*, 1996; *Torsvik et al.*, 1998]. The variety of dyes used in these studies (acridine orange, Hoechst 3342, PO-PRO-3, DAPI, Syto-ll, Syto-59, Arch344-FITC, and Bac388-TRITC) suggests that either nucleic acid and ribosome specific dyes universally bind with clays, or that the dyes are binding with complex organic molecules where tubes invade the glass. Even so, the fluorescence of a single dye should be viewed with caution if it is not supported by other evidence such as the colocation of carbon and other elements essential for life [e.g., *Furnes et al.*, 2001].

[40] Acridine orange (AO), which was used in this study, also binds to clays such as saponite [*Garfinkel-Shweky and Yariv*, 1997a], beidellite

[*Garfinkel-Shweky and Yariv*, 1999], montmorillonite, laponite and vermiculite [*Garfinkel-Shweky and Yariv*, 1997b; *Yariv et al.*, 1989]. The adsorption of cationic dyes on clays has been proposed as a model for interactions between organic compounds and these minerals [*Neumann et al.*, 2000]. AO can be found in the interlayer spaces of clays with their aromatic rings lying parallel to the silicate layers, so the dye can concentrate in regions of alteration that are also proposed to be the areas colonized by microbial life.

[41] AO can produce false positives when clay is present, however, the AO signals produced in the HSDP 531-5.9 suggest that nucleic acids are present. The two images in Figure 4 show the location of smectite that rims the bubble (vesicle) in basalt glass (Figure 4a) and the location of fluorescence within the clay and glass. The sharp boundary between glass and smectite is evident by the transition from low background fluorescence in the glass to moderate background fluorescence due to nonspecific binding to clay within the smectite layer (Figure 4b). Within the smectite are zones of fluorescence composed of round, green, 1-μm-diameter spheres similar to the distribution of cells seen in smectite from Columbia River basalts [*McKinley et al.*, 2000]. These zones are above background, are roughly parallel to the glass surface, and are 5 and 10 μm from the glass. Within these zones some strings of fluorescence spheres could be cells.

[42] When AO is bound to DNA and illuminated with UV, it emits at 536 nm (green) and when it is bound to RNA or single stranded DNA it emits at 650 nm (red). Within the smectite (Figure 4b) most of the cell-like features fluoresce green. At the
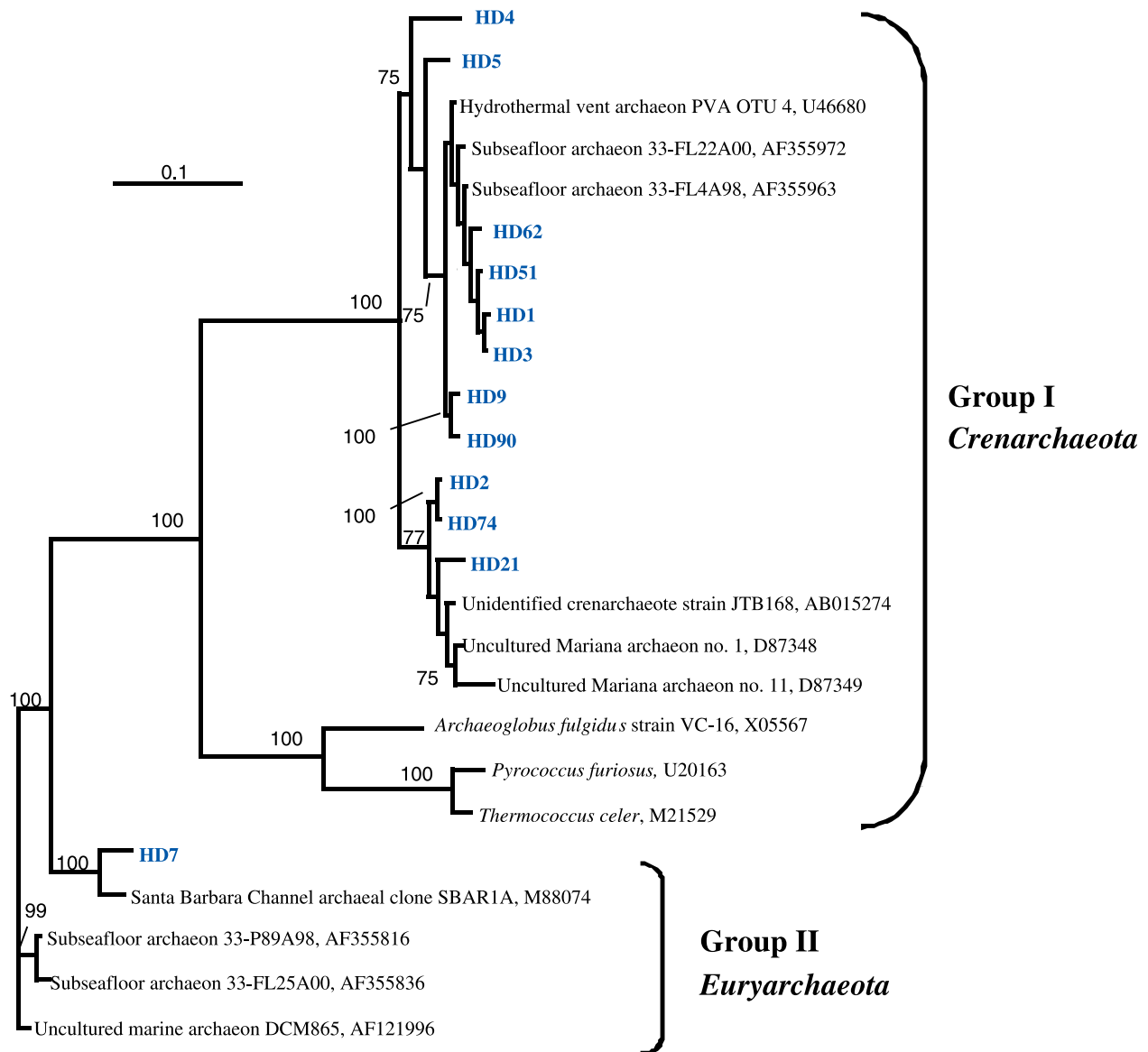
Figure 8. Phylogenetic affiliations of HSDP core R530-9.8 archaeal clones to close relatives based on 610 base pairs of aligned 16S rDNA sequences. The neighbor-joining tree was constructed using the Kimura 2-parameter distance method [*Swofford*, 2001]. The numbers at the nodes indicate the bootstrap confidence values expressed as percentages of 1,000 bootstrap replications. Bootstrap values of less than 50% are not shown. The scale bar represents 0.1 estimated changes per nucleotide. HD indicates the Hawaiian Drill clones. All clones but HD7 are most closely related to clones from deep sea vents, the oceanic subsurface, and deep sea sediment. HD7 is most closely related to a clone isolated from water in the Santa Barbara Basin.

interface of the glass and the smectite, however, both red and green fluorescence can be found. Also, where tubes have penetrated the glass and are exposed on the surface of the thin section, both colors of fluorescence are present (Figure 4b). This suggests that both DNA and RNA (or degraded, single-stranded DNA) is present within the smectite and the tubes that penetrate glass. The association of epifluorescence with the tubes and the localized fluorescence above background in the clay, the rounded shapes, the formation of chains and clusters, and the color spectra (green to red) is suggestive of microbial cells or of fossil cells within the tubes (Figure 4b). The region of AO

fluorescence in the smectite rim of the vesicle is identical to the area examined with UV induced fluorescence and Raman spectroscopy as discussed in the next section.

4.3. Deep Ultraviolet Native Fluorescence

[43] Laser-induced native fluorescence search strategies rely on direct excitation of naturally occurring microbial chromophores and do not require the introduction of tagging fluorophores. Such native fluorescence techniques have been widely employed in both laboratory and field work and remain the gold standard for sensitivity [*Asher*, 1993; *Elliot*, 1995]. A variety of ring compounds essential to microorganisms including the aromatic amino acids, the nucleic acids, flavins, and quinones exhibit strong native fluorescence response to excitation between 200 and 280 nm [*Cary*, 1982; *Grasselli and Bulkin*, 1991]. Mercury lamp excitation at 254 nm can elicit native fluorescent activity in the bacterium *Escherichia coli* [*Glazier and Weetall*, 1994] and excitation at 230 nm produces native fluorescence in algae and phytoplankton [*Determann et al.*, 1998].

[44] The routine use of deep UV excitation to obtain native fluorescence biosignatures from microorganisms and their metabolic products is now feasible due to the development of lightweight, inexpensive hollow cathode ion lasers emitting photons in the 200 to 250 nm range [*Storrie-Lombardi et al.*, 2001]. The lasers employed in this study operate at 224.3 nm and 248.6 nm wavelengths. Excitation at 224.3 nm falls within the absorption bands for the aromatic amino acids. Excitation at 248.6 nm falls within the absorption bands for both the nucleic acids and the aromatic amino acids, particularly tryptophan.

[45] This native fluorescence response can serve as an initial biomolecule detection probe and provide coregistered morphological (size and shape) and chemical (fluorescence) information. This method only provides minimal chemical specificity to aid in identification of the target, so for more detailed chemical information we investigated the regions

exhibiting laser-induced native fluorescence with deep UV resonance Raman spectroscopy.

4.4. Resonance Raman Spectroscopy

[46] The high information content of Raman spectra and minimal sample preparation required make Raman spectroscopy extremely attractive as a monitoring technique for a wide variety of biochemical reactions [*Spiro*, 1987], determining the molecular structure of viral protein [*Wen et al.*, 1997], and characterizing the chemistry of soils and minerals [*Wang et al.*, 1995]. The technique has been proposed for in situ mineralogical and paleontological exploration of the Martian regolith [*Wang et al.*, 1999].

[47] Raman spectroscopy [*Raman and Krishnan*, 1928] characterizes molecular bond vibrations by measuring the exchange of energy between the bond and incident light. The exchange of energy is observed as a change (shift) in the wavelength of scattered light compared to incident light, which is referred to as the Raman shift. Each bond type results in a Raman shift, and a Raman spectrum is a plot of the intensity of scattered light vs. Raman shift (Figure 6). This method can provide quantitative information about all the organic and inorganic molecular species in a sample. Because the Raman spectra uniquely identify the composition of samples, they are often referred to as "fingerprints."

[48] The Raman event is typically an inefficient phenomenon (signal to noise $<10^{-9}$) and early attempts to produce Raman spectra of bacteria with visible light excitation were unsuccessful due to fluorescence interference [*Dalterio et al.*, 1987]. However, deep ultraviolet (UV) laser excitation within the absorption bands (200–280 nm) of the nucleic acids, aromatic amino acids, and quinones can produce *resonance* Raman events with an increase in signal strength by as much as 10^8 [*Asher*, 1993]. Consequently, UV resonance Raman (UVRR) spectroscopy has been employed to investigate nucleic acids [*Fodor et al.*, 1985], the secondary structure of DNA [*Perno et al.*, 1989], the aromatic amino acids [*Johnson et al.*, 1986],

and alterations in oxidation state, electronic excited states, and peptide conformation [*Asher et al.*, 1991; *Rodgers et al.*, 1992].

[49] UVRR is an extremely sensitive method of detecting microorganisms. Excitation in the 200–257 nm range produces clear UV resonance Raman spectra for a variety of bacteria and spores blueward of the concurrent fluorescence [*Manoharan et al.*, 1990; *Nelson et al.*, 1992]. The technique is sensitive enough to detect less than 1 ppm concentrations of aromatic and polycyclic aromatic hydrocarbons in aqueous solution [*Sparrow et al.*, 2001]. Deep UV resonance Raman techniques have been demonstrated to have an in situ detection limit of about 60 ppb or about 20 microorganisms against plagioclase and calcite backgrounds [*Storrie-Lombardi et al.*, 2001], and the technique has been proposed for life detection experiments on Mars [*Storrie-Lombardi et al.*, 1999].

[50] The deep UV resonance Raman spectrum (Figure 6) of the region exhibiting fluorescence activity in Figure 5e contains evidence of homocyclic and heterocyclic unsaturated ring structures. Raman activity red-ward (to the right) of 1000 wave numbers is most often associated with biomolecular rather than mineral targets [*Storrie-Lombardi*, 1997]. Activity near 1600 wave numbers can be assigned to phenyl ring vibration of tryptophan ($1614–1622$ cm^{-1}), in-plane ring stretching of tyrosine ($1613–1617$ cm^{-1}), the in-plane ring stretching and bending of guanine (1603 cm^{-1}), and the ring mode stretching of guanine ($1575–1580$ cm^{-1}) and of adenine ($1580–1581$ cm^{-1}) [*Perno et al.*, 1989; *Asher et al.*, 1991]. Activity around $1549–1555$ cm^{-1} can often be attributed to symmetric stretching of tryptophan's indole ring [*Asher*, 1993; *Asher et al.*, 1991]. Cytosine ring mode stretching appears near 1527 cm^{-1}. Purine ring bond stretching is particularly prominent for guanine at $1485–1489$ cm^{-1} and for adenine at $1336–1339$ cm^{-1}. Activity arising from tryptophan's pyrrole ring vibration also occurs at $1340–1350$ cm^{-1}. Tyrosine symmetric stretch activity appears at $1209–1210$ cm^{-1} and tyrosine's in-plane CH bend can be seen at $1178–1180$ cm^{-1}. The symmetric ring stretch of tryptophan's benzene and pyrrole arises

at $1006–1016$ cm^{-1}. [*Spiro*, 1987] The UVRR spectrum for our sample of the Hawaiian deep basalt has significant Raman shifts in this organic fingerprint region.

[51] The location of mineral and water peaks in the Raman spectrum for this sample do not coincide with the organic fingerprint region. The Raman activity attributed to silicates at 470 cm^{-1} and the activity from olivine at 800 cm^{-1} is expected for this olivine phyric glassy basalt. Although calcite was not observed in this sample, the activity attributable to calcite at 1086 cm^{-1} is not surprising since it exhibits an extremely large Raman cross-section at this laser wavelength [*Storrie-Lombardi et al.*, 2001]. The phosphate activity at 949 cm^{-1} is interesting in light of the electron microprobe and EDS findings of phosphorus concentrations at some smectite-glass boundaries and the report of secondary apatite ($Ca_5(PO_4)_3$(F, Cl, OH)) in smectite of some samples from HSDP [*Walton and Schiffman*, 2003]. The broad regions of activity around 2300 cm^{-1} from $-CH$ stretching are to be expected in a colonized rock matrix, and the water fingerprint at 3100 to 3400 cm^{-1} is likely to be due to water that makes up 10% or more of the smectite.

4.5. Environmental Scanning Electron Microscopy (ESEM)

[52] The UV LINF images, the UVRR spectra, and the AO staining suggest that there is biological material in the rims of vesicles within Unit 198. Figure 7 shows a vesicle edge, where the smectite layer (left, textured) meets the glass (right, smooth). Cell-like bodies are present in the smectite layer that has broken away from the glass (Figure 7a). On the glass surface are spheroids that appear to be mineralized with clays. The presence of organic material in the spheres was confirmed by energy dispersive analysis (EDS) that showed a contrasting chemistry between the mineralized cells, clays alone, and the glass. Figures 7b and 7c are enlargements of the rectangles delineated in Figure 7a. In Figure 7a two mineralized spheroids (one of which could have been dislodged from a pit in the glass) lie on the glass surface. Figure 7c shows two abutting clay-covered spheres,

one of which has an elongated protrusion (at its left). The EDS analysis of these spheres, revealing an abundance of C, P, Mg, and Cl, all elements commonly associated with biotic systems, provides further evidence that these forms are most likely microbial cells.

[53] These ESEM images presented here, together with other observations (not shown) of burrows in the glass and burrows which have cell-shaped, clay-covered bodies inside them imply that microorganisms are present and that they play a role in clay formation within these glasses. The ESEM evidence supports the hypothesis that microorganisms are present near the smectite-glass interface.

4.6. Amino Acids

[54] The amino acids serine, glycine, alanine, and valine are the only amino acids detected in the rock (Table 2). The standard deviation for L-serine is high relative to the detected concentration, so the detection of this amino acid should be taken as very tentative. Free amino acid concentrations in seawater can range from 50–100 nM in the open Pacific to 500 nM or more in bay waters [Lee and Bada, 1977]. The total amino acid concentration in the current rock sample is around 0.1 nmol, an amount that could be contributed by a few ml of seawater per gm of rock.

[55] No D-serine or D-valine was detectable above the background, but D-alanine was detected at very low concentrations. The observed D/L ratio for alanine (D/L Ala) is 0.1 ± 0.08. This ratio is consistent with that seen in living microbial cultures as a result of D-alanine in bacterial cell walls. Some minor contribution to the concentration of D-alanine from racemization in dead cells is also possible. D/L Ala in Pacific Ocean water ranges from 0.1 in open ocean surface water [Lee and Bada, 1977] to 0.2 in nearshore waters [Bada et al., 1982]. The D/L Ala values measured in this study are on the low end of this range. This suggests that the D-alanine levels inside the rock are kept lower than those of the surrounding seawater by active amino acid metabolism in living microorganisms within the rock.

[56] Of further interest is the absence of aspartic acid and glutamic acid, two amino acids normally seen in any biological or environmental sample. This could be due to an artifact of the sample processing, either selective retention by the clays or selective destruction due to catalysis by the clays during the acid extraction. Similar effects have been observed on acid extraction of amino acids from palagonite (G. D. McDonald, unpublished data, 2002). An alternative explanation for the absence of aspartic and glutamic acids is selective decomposition in the sample prior to analysis, due to chemical and/or biological processes. Overall, the amino acid profile observed in the basalt is not inconsistent with a biological source, but there may have been some post-biological alteration of the amino acids. The profile may indicate that exogenous amino acids are present, however, in small amounts. If all the amino acids extracted from the rock were due to living organisms, then there would be about 10^5 cells per gram of rock.

4.7. 16S rDNA Amplification

[57] Multiple attempts using several different primer sets failed to amplify bacteria, which indicates that our lack of amplification success was not simply due to primer bias. A nested PCR approach achieved only faint amplification of bacteria (data not shown). One possible explanation for these results is that bacterial cells may not be as abundant as archaea in the drill core sample. Analysis of the total biomass of archaea and bacteria with PCR-independent approaches such as phospholipid fatty acid analysis (PLFA) or fluorescence in situ hybridization (FISH) would be necessary to determine the relative abundance of these organisms in the core material.

[58] All of the clones obtained form the rock, with the exception of the Euryarchaeal clone HD7, were closely related (97 to 99% similar) to Group I marine Crenarchaea identified from similar deep-sea habitats (Figure 8). This suggests that contamination of this sample was at a minimum during both sample handling and subsequent DNA analysis. Therefore we propose that the organisms identified from this analysis represent archaea that

are resident to the core material collected from 1351 m depth. The presence of one archaeal clone that is similar to an organisms identified from the water on the Santa Barbara Basin off California suggests that this organism was introduced into the basalt by pumping of seawater into the hole while drilling or by subsequent handling or washing of the basalt. Parallel analysis of the water used in these processes was not possible, as samples of this fluid were not retained. However, future studies should include analysis of the drill fluids to unequivocally determine the origin of the sequences retrieved from deep drill cores.

[59] The technique used for extracting DNA from the rocks is extremely sensitive and has the potential for amplifying just a few copies of genes extracted from the rock. Thus the sensitivity for detecting DNA is within the limits of the number of cells per gram of rock ($<10^5$ cells/g) indicated by the amino acid analysis.

4.8. Contamination of Subsurface Samples

[60] HSDP drilling was undertaken to understand the geological evolution of Hawaii and the Hawaiian Islands. The microbiology of the subsurface was not considered during drilling, and no tests of the microbial content of the drilling fluid were made. Drilling, no doubt, introduces contamination into the cores [Smith et al., 2000], and cores were handled and then stored exposed to the air so there were additional opportunities for contamination.

[61] Our data provide evidence for life in the HSDP core, but which of the data are evidence for in situ subsurface life and which data can be explained by contamination needs to be evaluated. Our analyses can be divided into those that were applied to bulk samples (DNA and amino acid extraction) and those that were applied to precisely located regions in the interior of the core. Chemical signals of life extracted from bulk samples could be due to pervasive contamination of the rocks, although we explain below why we believe this is not the case for the DNA and amino acid analyses. The precisely located chemical evidence could also be a consequence of contamination if

the contaminants lodge in areas where the physical evidence of life is also present. The physical evidence (tubes and cell-like objects), however, is not subject to modification by contamination. Our data can be subjectively ranked according to whether they are evidence for in situ life and whether they could be the result of contamination.

[62] Amino acids and nucleic acids are clear evidence for life and these were identified by four techniques, DNA extraction, UVRR spectroscopy, OA staining, and amino acid extraction. We rank DNA extracted from the interiors of bulk samples and identified by UVRR as most likely indicators of indigenous microorganisms in the rocks. We consider the extracted DNA to be a strong indicator because the majority of the DNA from the rock is most closely related to organisms from the subsurface ocean crust and hydrothermal vents, and the one outlier is clearly identified as such. UVRR spectroscopy is a strong indicator of indigenous microorganisms because for the nucleic acid and amino acid spectrum to be the consequence of contamination would require that the organic compounds be introduced into and preserved in the smectite at the edge of the vesicle, but not deposited along the interior wall of the vesicle. This UVRR evidence is corroborated by AO stain that suggests cells are present in the smectite, by the presence of tubes (similar to those attributed to microbes in other rocks) that start near smectite and penetrate into glass, and by native fluorescence in the smectite. Amino acids extracted from the bulk sample are also indicative of life, but their low levels make it possible that this signal represents contamination of the rock. Thus the most compelling evidence of indigenous life in the rocks are the UVRR spectrum and extracted DNA. The UVRR spectrum is supported by native fluorescence and nucleic acid staining.

[63] Our other observations are compatible with the presence of life in the core. These are the distribution of tubes, the ESEM images, and the distribution of P and C in the rims of vesicles. Alteration of glass is a slow process and the tubes were present when the rocks were collected. Also,

these tubular features in the glass appear similar to those found in basalts collected from the deep sea and which have been attributed to microorganisms. The presence of nucleic acids in the tubes and the similarities of the tubes in the Hawaii rocks and tubes in deep sea rocks further suggest microorganisms were present when the tubes were formed. The ESEM images and the distribution of P and C in the sample are supportive of the presence of life but the presence of apatite in some samples and the suggestion that carbonate is present (on the basis of UVRR) makes the P and C measurements less valuable for indicating the presence of life in the rocks.

[64] The data we feel in strongest agreement with the hypothesis that life existed in the rocks before they were drilled are: (a) the location and style of tubes within glass (Figure 2), (b) UV Raman spectroscopy (Figure 6), and (c) nucleic acid identification (Figure 8). The ESEM images, native fluorescence, elemental maps, AO staining, and amino acid extraction are supporting evidence, but are not sufficient in themselves to indicate indigenous life in the Hawaiian subsurface. Physical features (cells and tubes) are certainly not the result of contamination. Most DNA clones are compatible with subsurface ocean environments and therefore appear indigenous to the Hawaiian subsurface. If the organic compounds located by UVRR and AO were introduced by contamination, they would be expected to be present in the interior of vesicles and other open spaces in the rock, but they are present within the smectite and glass and absent for the void space. The only data that could be attributed to contamination are the amino acids extracted from the bulk sample, however, the absence of certain amino acids from the extract suggests that even this signal is not due to contamination of the rock with seawater.

4.9. Hawaiian Subsurface Biosphere

[65] Results from deep drilling on Hawaii indicate that conditions are suitable for microbial habitation to depths of at least three kilometers at the margin of the island. Above three kilometers temperatures are less than 50°C and fluid flow could maintain a

supply of nutrients such as organic compounds and inorganic oxidants and reductants as deep as 2400 m into the volcano. Microbial invasion of the subsurface is apparent in the hyaloclastites that make up about one third of the three-kilometer section drilled by HSDP. Hyaloclastites are also exposed in the headwalls of some of the giant underwater landslides on the flanks of the Hawaiian Islands [*Clague and Moore*, 2002], so hyaloclastites may represent a significant portion of the basement of this and other volcanic islands. The evidence for microorganisms within HSDP hyaloclastites and the potential mediation of the alteration of rocks by microorganisms suggests that the microbes can change the physical properties of the hyaloclastites. If the net result of the activity of the microbes is to weaken the hyaloclastites, then the microbial activity may be linked to the landslides. Alternatively, infilling of pore space will restrict fluid flow at depth, limit microbial activity, and cement the hyaloclastite and consequently strengthen the foundation of the volcano.

5. Conclusions

[66] In previous studies evidence of microbial activity has been documented in drill cores in basalts from depths of 550 m. The data presented here from the Hawaii Scientific Drilling Program (HSDP) indicates that evidence for life can be extracted from drill holes to at least a depth of 1353 meters. Optical evidence for microbial activity in the Hawaiian Drill Core indicates that microbes were present in rocks to depths of 1895 m.

[67] The results of multiple analytical techniques support the hypothesis that microorganisms are present in the boundary between primary volcanic glass and secondary clay in subsurface Hawaiian hyaloclastites. We examined only one lithologic unit with the complete set of techniques, but on the basis of the petrographic examination of other units, it appears that microorganisms are, or were, present from 1080 m to 1895 m and possibly deeper.

[68] Excitation of native fluorescence with deep UV lasers is a powerful technique for the rapid in

situ detection of regions most likely to contain complex organic molecules. Deep UV resonance Raman spectroscopy can confirm in situ the presence of double bond ring structures in biomolecules such as the nucleic acids and the aromatic amino acids. Both techniques can be employed with limited sample preparation and without staining. In the current study the isolation of highly fluorescent regions following 224.6 nm laser excitation led to the detection of a $1300-1600$ cm^{-1} deep UV resonance Raman biosignature following excitation of the same target at 248.6 nm. Coregistration of these signatures led to an ESEM search for and identification of morphological forms resembling a known class of deep sea microorganisms. Wavelength dispersive electron microprobe mapping of the surface documented significant elevations in carbon, phosphorous, chloride, sulfur, calcium and magnesium in the region of these coccoid structures that would be expected in the presence of microbial life. Deep UV fluorescence imaging and resonance Raman spectral techniques appear well-suited for exploration of subsurface deep core material. The dominance of archaeal DNA in the clone sequences obtained from the unit we examined, and the presence of only a single clone of an organism likely to be derived from seawater suggests that the most DNA sequences represent organisms in the rocks at the time they were collected.

Acknowledgments

References

Altschul, S. F., W. Gish, W. Miller, E. W. Myers, and D. J. Lipman, Basic local alignment search tool, *J. Mol. Biol.*, *215*, 403–410, 1990.

Asher, S. A., UV resonance Raman spectroscopy for analytical, physical, and biophysical chemistry. 1, *Anal. Chem.*, *65*, A59–A66, 1993.

Asher, S. A., P. J. Larkin, and J. Teraoka, Ultraviolet resonance Raman and absorption difference spectroscopy of myoglobins—Titration behavior of individual tyrosine residues, *Biochem. U.S.*, *30*, 5944–5954, 1991.

Bada, J. L., E. Hoopes, and M. Ho, Combined amino acids in Pacific Ocean waters, *Earth Planet. Sci. Lett.*, *58*, 276–284, 1982.

Bada, J. L., D. P. Glavin, G. D. McDonald, and L. Becker, A search for endogenous amino acids in Martian meteorite ALH84001, *Science*, *279*, 362–365, 1998.

Cary, P. R., *Biochemical Applications of Raman and Resonance Raman Spectroscopy*, Academic, San Diego, Calif., 1982.

Clague, D. A., and J. G. Moore, The proximal part of the giant submarine Wailau Landslide, Molokai, Hawaii, *J. Volcanol. Geotherm. Res.*, *113*, 259–287, 2002.

Dalterio, R. A., W. H. Nelson, D. Britt, and J. F. Sperry, An ultraviolet (242 nm excitation) resonance Raman study of live bacteria and bacterial component, *Appl. Spectrosc.*, *41*, 417–422, 1987.

DeLong, E. F., T. L. Taylor, L. T. Marsh, and C. M. Preston, Visualization and enumeration of marine planktonic archaea and bacteria by using polyribonucleotide probes and fluorescent in situ hybridization, *Appl. Environ. Microbiol.*, *65*, 5554–5563, 1999.

Determann, S., J. M. Lobbes, R. Reuter, and J. Rullkotter, Ultraviolet fluorescence excitation and emission spectroscopy of marine algae and bacteria, *Mar. Chem.*, *62*, 137–156, 1998.

Elliot, D. J., *Ultraviolet Laser Technology and Applications*, Academic, San Diego, Calif., 1995.

Fisk, M. R., S. J. Giovannoni, and I. H. Thorseth, The extent of microbial life in the volcanic crust of the ocean basins, *Science*, *281*, 978–980, 1998.

Fisk, M. R., I. H. Thorseth, E. Urbach, and S. J. Giovannoni, Investigation of microorganisms and DNA from rock and thermal waters of Ocean Drilling Program Site 1026, *Proc. Ocean Drill. Program Sci. Results*, *168*, 167–174, 2000.

Fisk, M. R., M. C. Storrie-Lombardi, S. Douglas, and R. Popa, Microorganisms from a depth of 1350 m in Hawaii (abstract), *Eos Trans. AGU*, *82*(47), Fall Meet. Suppl., Abstract B22D-0179, 2001.

Fodor, S. P. A., R. P. Rava, T. R. Hayes, and T. G. Spiro, Ultraviolet resonance Raman spectroscopy of the nucleotides with 266 nm, 240 nm, 218 nm, and 200 nm pulsed laser excitation, *J. Am. Chem. Soc.*, *107*, 1520–1529, 1985.

Furnes, H., and H. Staudigel, Biological mediation in ocean crust alteration: How deep is the deep biosphere?, *Earth Planet. Sci. Lett.*, *166*, 97–103, 1999.

Furnes, H., I. Thorseth, O. Tumyr, T. Torsvik, and M. Fisk, Microbial activity in the alteration of glass from pillow lavas from Hole 896A, *Proc. Ocean Drill. Program Sci. Results*, *148*, 191–206, 1996.

Furnes, H., K. Muehlenbachs, O. Tumyr, T. Torsvik, and I. Thorseth, Depth of bio-alteration in the ocean crust: Costa Rica Rift (Hole 504B), *Terra Nova*, *11*, 228–233, 1999.

Furnes, H., H. Staudigel, I. Thorseth, T. Torsvik, K. Muehlenbachs, and O. Tumyr, Bioalteration of basaltic

glass in the ocean crust, *Geochem. Geophys. Geosyst.*, *2*, Paper number 2000GC000150, 2001.

Garfinkel-Shweky, D., and S. Yariv, Metachromasy in clay-dye systems: The adsorption of acridine orange by Na-saponite, *Clay Miner.*, *32*, 653–663, 1997a.

Garfinkel-Shweky, D., and S. Yariv, The determination of surface basicity of the oxygen planes of expanding clay minerals by acridine orange, *J. Colloid Interface Sci.*, *188*, 168–175, 1997b.

Garfinkel-Shweky, D., and S. Yariv, Metachromasy in clay dye systems: The adsorption of acridine orange by Na-beidellite, *Clay Miner.*, *34*, 459–467, 1999.

Giovannoni, S. J., M. R. Fisk, T. D. Mullins, and H. Furnes, Genetic evidence for endolithic microbial life colonizing basaltic glasses/seawater interfaces, *Proc. Ocean Drill. Program Sci. Results*, *148*, 207–214, 1996.

Glavin, D. P., J. L. Bada, K. L. F. Brinton, and G. D. McDonald, Amino acids in the Martian meteorite Nakhla, *Proc. Natl. Acad. Sci. U. S. A.*, *96*, 8835–8838, 1999.

Glazier, S. A., and H. H. Weetall, Autofluorescence detection of Escherichia coli on silver membrane filters, *J. Microbiol. Methods*, *20*, 23–27, 1994.

Gold, T., The deep, hot biosphere, *Proc. Natl. Acad. Sci. U. S. A.*, *89*, 6045–6049, 1992.

Grasselli, J. G., and B. J. Bulkin, *Analytical Raman Spectroscopy*, John Wiley, New York, 1991.

Hall, T., BioEdit sequence alignment editor, Dept. of Microbiol., N. C. State Univ., Raleigh, 2000.

Hawaii Scientific Drilling Project-2, Core logs and summarizing data, edited by C. A. Seaman, M. O. Garcia, and E. M. Stolper, Calif. Inst. of Technol., Pasadena, Calif., 2000.

Huber, J. A., D. A. Butterfield, and J. A. Baross, Temporal changes in archaeal diversity and chemistry in a mid-ocean ridge seafloor habitat, *Appl. Environ. Microbiol.*, *68*, 1585–1594, 2002.

Israel, E. J., R. E. Arvidson, A. Wang, J. D. Pasteris, and B. L. Jolloff, Laser Raman spectroscopy of varnished basalt and implications for in situ measurements of Martian rocks, *J. Geophys. Res.*, *102*, 28,705–28,716, 1997.

Johnson, C. R., M. Ludwig, and S. A. Asher, Ultraviolet resonance Raman characterization of photochemical transients of phenol, tyrosine, and tryptophan, *J. Am. Chem. Soc.*, *108*, 905–912, 1986.

Kato, C., L. Li, J. Tamaoka, and K. Horikoshi, Molecular analyses of the sediment of the 11,000-m deep Mariana Trench, *Extremophiles*, *1*, 117–123, 1997.

Kemp, P. F., B. F. Sherr, E. B. Sherr, and J. J. Cole, *Handbook of Methods in Aquatic Microbial Ecology*, Lewis, Boca Raton, Fla., 1993.

Kimura, M., A simple method for estimating evolutionary rates of base substitution through comparative studies of nucleotide sequences, *J. Mol. Evol.*, *16*, 111–120, 1980.

Lee, C., and J. L. Bada, Dissolved amino acids in equatorial Pacific, Sargasso Sea, and Biscayne Bay, *Limnol. Oceanogr.*, *22*, 502–510, 1977.

Li, L., C. Kato, and K. Horikoshi, Microbial diversity in sediments collected from the deepest cold-seep area, the Japan Trench, *Mar. Biotechnol.*, *1*, 391–400, 1999.

Lockwood, J. P., and P. W. Lipman, Holocene eruptive history of Mauna Loa volcano, *U.S. Geol. Surv. Prof. Pap.*, *1350*, 509–535, 1987.

Manoharan, R., E. Ghiamati, R. A. Dalterio, K. A. Britton, W. H. Nelson, and J. F. Sperry, UV resonance Raman spectra of bacteria, bacterial spores, protoplasts and calcium dipicolinate, *J. Microbiol. Methods*, *11*, 1–15, 1990.

Massana, R., A. E. Murray, C. M. Preston, and E. F. DeLong, Vertical distribution and phylogenetic characterization of marine planktonic archaea in the Santa Barbara Channel, *Appl. Environ. Microbiol.*, *63*, 50–56, 1997.

McDonald, G. D., and J. L. Bada, A search for amino acids in the Martian meteorite EETA79001, *Geochim. Cosmochim. Acta*, *59*, 1179–1184, 1995.

McKinley, J. P., T. O. Stevens, and F. Westall, Microfossils and paleoenvironments in deep subsurface basalt samples, *Geomicrobiol. J.*, *17*, 1–12, 2000.

Moore, J. G., B. L. Ingram, K. R. Ludwig, and D. A. Clague, Coral ages and island subsidence, Hilo drill hole, *J. Geophys. Res.*, *101*, 11,599–11,605, 1996.

Moyer, C. L., J. M. Tiedje, F. C. Dobbs, and D. M. Karl, Diversity of deep-sea hydrothermal vent Archaea from Loihi Seamount, Hawaii, *Deep Sea Res., Part II*, *45*, 303–317, 1998.

Nelson, W. H., R. Manoharan, and J. F. Sperry, UV resonance Raman studies of bacteria, *Appl. Spectrosc. Rev.*, *27*, 67–124, 1992.

Neumann, M. G., F. Gessner, A. P. P. Cione, R. A. Sartori, and C. C. S. Cavalheiro, Interaction between dyes and clays in aqueous suspension, *Quimica Nova*, *23*, 818–824, 2000.

Parkes, R. J., B. A. Cragg, S. J. Bale, J. M. Getliff, K. Goodman, P. A. Rochelle, J. C. Fry, A. J. Weightman, and S. M. Harvey, Deep bacterial biosphere in Pacific Ocean sediments, *Nature*, *371*, 410–413, 1994.

Perno, J. R., C. A. Grygon, and T. G. Spiro, Ultraviolet Raman excitation profiles for the nucleotides and for the nucleic acid duplexes poly(RA), poly(RU) and poly(DG-DC), *J. Phys. Chem.*, *93*, 5672–5678, 1989.

Raman, C. V., and K. S. Krishnan, A new type of secondary radiation, *Nature*, *121*, 501–502, 1928.

Rodgers, K. R., C. Su, S. Subramanian, and T. G. Spiro, Hemoglobin R-T structural dynamics from simultaneous monitoring of tyrosine and tryptophan time-resolved UV resonance Raman signals, *J. Am. Chem. Soc.*, *114*, 3697–3709, 1992.

Romeis, B., *Mikroskopische Technik*, edited by J. C. Stockert and J. A. Lisanti, Oldenbourg Verlag, Munich, Germany, 1968.

Sambrook, J., E. F. Fritsch, and T. Maniatis, *Molecular Cloning*: *A Laboratory Manual*, 2nd ed., Cold Spring Harbor Lab., Cold Spring Harbor, N. Y., 1989.

Shapiro, H. M., *Practical Flow Cytometry*, A. R. Liss, New York, 1988.

Sharp, W. D., B. D. Turrin, P. R. Renne, and M. A. Lanphere, The $^{40}Ar/^{39}Ar$ and K/Ar dating of lavas from the Hilo 1-km core hole, Hawaii Scientific Drilling Project, *J. Geophys. Res.*, *101*, 11,593–11,598, 1996.

Smith, D. C., A. J. Spivack, M. R. Fisk, S. A. Haveman, and H. Staudigel, Tracer-based estimates of drilling-induced microbial contamination of deep sea crust, *Geomicrobiol. J.*, 17, 207–219, 2000.

Sparrow, M. C., J. F. Jackovitz, C. H. Munro, W. F. Hug, and S. A. Asher, A new 224 nm hollow cathode UV laser Raman spectrometer, *J. Appl. Spectrosc.*, 55, 66–70, 2001.

Spiro, T. G., (Ed.), *Biological Applications of Raman Spectroscopy*, vol. I–III, John Wiley, New York, 1987.

Stahl, D. A., and R. I. Amann, Development and application of nucleic acid probes, in *Nucleic Acid Techniques in Bacterial Systematics*, edited by E. Stackebrandt and M. Goodfellow, pp. 205–248, John Wiley, New York, 1991.

Stevens, T. O., and J. P. McKinley, Lithoautotrophic microbial ecosystems in deep basalt aquifers, *Science*, 270, 450–454, 1995.

Stockert, J. C., and J. A. Lisanti, Acridine-orange differential fluorescence of fast- and slow-reassociating chromosomal DNA after in situ DNA denaturation and reassociation, *Chromosoma*, 37, 117–130, 1972.

Stolper, E. M., D. J. DePaolo, and D. M. Thomas, The Hawaii Scientific Drilling Project: Introduction to the special section, *J. Geophys. Res.*, 101, 11,593–11,598, 1996.

Stolper, E. M., D. J. DePaolo, and D. M. Thomas, Hawaii Scientific Drilling Project: Overview of project goals and stratigraphy, *Eos Trans. AGU*, 81(48), Fall Meet. Suppl., Abstract V11D-01, 2000.

Storrie-Lombardi, M. C., Raman databases, Bayesian pattern matching, and nonlinear artificial neural networks, paper presented at JPL/Caltech in Situ Workshop on Raman Spectroscopy, Jet Propul. Lab., Pasadena, Calif., 1997.

Storrie-Lombardi, M. C., A. I. Tsapin, G. D. McDonald, H. Sun, and K. H. Nealson, Ultraviolet Raman spectroscopy for in situ geobiological exploration of Mars, *Am. Chem. Soc. Abstr. Pap.*, 217, 069-GEOC, 1999.

Storrie-Lombardi, M. C., W. F. Hug, G. D. McDonald, A. I. Tsapin, and K. H. Nealson, Hollow cathode ion lasers for deep ultraviolet Raman spectroscopy and fluorescence imaging, *Rev. Sci. Instrum.*, 72, 4452–4459, 2001.

Sun, H., E. I. Friedmann, G. D. McDonald, and K. H. Nealson, Organic biosignatures in Antarctic sandstone, paper presented at 1st Astrobiology Science Conference, NASA Ames Res. Cent., Moffett Field, Calif., 2000.

Swofford, D. L., PAUP*: Phylogenetic Analysis Using Parsimony (*and Other Methods), Version 4, Sinauer Assoc., Sunderland, Mass., 2001.

Thomas, D. M., Hydrologic conditions deep within Mauna Kea volcano (abstract), *Eos Trans. AGU*, 81(48), Fall Meet. Suppl., Abstract V12C-06, 2000.

Thomas, D. M., F. L. Pailet, and M. E. Conrad, Hydrology of the Hawaiian Scientific Drilling Project borehole KP-1: 2. Groundwater geochemistry and regional flow patterns, *J. Geophys. Res.*, 101, 11,683–11,694, 1996.

Thorseth, I. H., H. Furnes, and M. Heldal, The importance of microbiological activity in the alteration of natural basaltic glass, *Geochim. Cosmochim. Acta*, 56, 845–850, 1992.

Thorseth, I., T. Torsvik, H. H. Furnes, and K. Muehlenbachs, Microbes play an important role in the alteration of oceanic crust, *Chem. Geol.*, 126, 137–146, 1995.

Torsvik, T., H. Furnes, K. Muehlenbachs, I. H. Thorseth, and O. Tumyr, Evidence for microbial activity at the glass-alteration interface in oceanic basalts, *Earth Planet. Sci. Lett.*, 162, 165–176, 1998.

Vergin, K. L., M. S. Rappe, and S. J. Giovannoni, Streamlined method to analyze 16S rRNA gene clone libraries, *BioTechniques*, 30, 938–944, 2001.

Walton, A. W., and P. Schiffman, Alteration of hyaloclastites in the HSDP 2 Phase 1 Drill Core: 1, Description and paragenesis, *Geochem. Geophys. Geosyst.*, 4(5), 8709, doi:10.1029/2002GC000387, 2003.

Wang, A., B. L. Jolliff, and L. A. Haskin, Raman spectroscopy as a method for mineral identification on lunar robotic exploration missions, *J. Geophys. Res.*, 100, 21,189–21,199, 1995.

Wang, A., B. L. Jolliff, and L. A. Haskin, Raman spectroscopic characterization of a highly weathered basalt: Igneous mineralogy, alteration products, and a microorganism, *J. Geophys. Res.*, 104, 27,067–27,077, 1999.

Wen, Z. Q., S. A. Overman, and G. J. Thomas, Jr., Structure and interactions of the single-stranded DNA genome of filamentous virus fd: Investigation by ultraviolet resonance Raman spectroscopy, *Biochemistry*, 36, 7810–7820, 1997.

Whitman, W. B., D. C. Coleman, and W. J. Wiebe, Prokaryotes: The unseen majority, *Proc. Natl. Acad. Sci. U. S. A.*, 95, 6578–6583, 1998.

Yariv, S., M. M. VonMoos, G. Kahr, and A. Rub, Thermal analytic study of the adsorption of Acridine-Orange by smectite minerals, *J. Therm. Anal.*, 35, 1997–2008, 1989.

Zhao, M., and J. L. Bada, Determination of a-dialkyl amino acids and their enantiomers in geological samples by HPLC after derivatization with a chiral adduct of 0-phthaldialehyde, *J. Chromatogr.*, 690, 55–63, 1995.